PCCP

Accepted Manuscript

This is an *Accepted Manuscript*, which has been through the Royal Society of Chemistry peer review process and has been accepted for publication.

Accepted Manuscripts are published online shortly after acceptance, before technical editing, formatting and proof reading. Using this free service, authors can make their results available to the community, in citable form, before we publish the edited article. We will replace this *Accepted Manuscript* with the edited and formatted *Advance Article* as soon as it is available.

You can find more information about *Accepted Manuscripts* in the Information for Authors.

Please note that technical editing may introduce minor changes to the text and/or graphics, which may alter content. The journal's standard Terms & Conditions and the Ethical guidelines still apply. In no event shall the Royal Society of Chemistry be held responsible for any errors or omissions in this *Accepted Manuscript* or any consequences arising from the use of any information it contains.

ROYAL SOCIETY OF CHEMISTRY

www.rsc.org/pccp

Journal Name RSCPublishing

ARTICLE

Electrochemical Flow-based Solution-Solid Growth of Cu_2O Nanorods Array: Potential Application to Lithium Ion Batteries

Cite this: DOI: 10.1039/x0xx00000x

Received 00th January 2012,
Accepted 00th January 2012

DOI: 10.1039/x0xx00000x

www.rsc.org/

Jeong Ho Shin[a], Sun Hwa Park[a], Seung Min Hyun[b], Jeong Won Kim[a,c], Hyun Min Park[a,c] and Jae Yong Song[a,c]*

The catalyzed solution-liquid-solid (SLS) growth has been well developed to synthesize semiconductor nanowires with controlled diameters. The SLS growth occurs in the longitudinal direction of nanowires, due to the directional anisotropy driven by the metal catalysts where chemical precursors are introduced. In present study, we report a selective, template-free, and environment-friendly electrochemical flow-based solution-solid (electrochemical flow-SS) growth of Cu_2O nanorods array. The anisotropy for directional growth without any catalysts is generated by the electrical field in a flowing electrolyte of ultra-dilute $CuSO_4$. The filamentary anisotropy originates from electric field enhancement on pyramidal nanocrystals in the electrolyte of low ionic conductivity (13 $\mu S \cdot cm^{-1}$). The Cu_2O and Cu nanorods are able to be selectively synthesized by controlling the electrolyte pH and oxygen dissolution into electrolyte. The synthesized Cu_2O nanorods array shows excellent electrochemical properties as an anode material for lithium-ion batteries; the specific capacities increase from 323 to 1206 $mA \cdot h \cdot g^{-1}$ during 500 cycles. The capacity enhancement is due to the phase transformation from Cu_2O to CuO, nano-restructuring of nanorods into fragmented nanoparticles, and the progressive generation of an electroactive polymeric gel-like layer on the surface of the nanoparticles. The electrochemical flow-SS growth of Cu_2O nanorods is expected to contribute to further development of other functional nanorods.

1 Introduction

Catalyst-mediated growths of one-dimensional nanocrystals without templates, such as solution-liquid-solid (SLS) and vapor-liquid-solid (VLS) methods, have been intensively investigated [1-4]. The catalysts create a directional anisotropy needed for one-dimensional growth, analogously to template-guided growth. Recently, a flow-SLS method, which utilizes the advantages of SLS and VLS growth, has been developed to grow CdSe-ZnSe heterostructured nanowires and the detailed characterization of growth mechanisms was unveiled due to its slow growth kinetics [4]. Previously, we reported an electrically filamentary growth of several nanorods such as Ag, Au, Cu and Ag-Cu alloy using a template-free electrodeposition in an ultra-dilute electrolyte [5]. In present study, we report an electrochemical flow-based solution-solid (electrochemical flow-SS) growth that Cu_2O and Cu nanorods arrays vertically aligned on substrate are selectively synthesized in a flowing aqueous electrolyte, mimicking the flow-SLS growth. The electric field generates a directional anisotropy in the flow of dielectric electrolyte without any catalysts, where the oxygen was supplied from the ambient.

Cu_2O was selected because, as a p-type semiconductor with a direct bandgap of 2.17eV, it has potential applications in energy conversion, photocatalysis, and gas sensors [6-8]. Until now, Cu_2O nanowires have been synthesized by vapor transport method, and liquid phase reduction method [9-11]. Generally, as Cu_2O is electrodeposited as thin films, due to the crystallographic isotropy of its primitive cubic crystal structure, nanotemplates are used for electrodeposition of Cu_2O nanowires [12]. And alkaline electrolytes including lactic acid or tartaric acid have typically been used because Cu_2O is stable in the pH range of 9 to 13, according to the Pourbaix diagram [13]. Therefore, it is a great challenge to electrodeposit Cu_2O nanorods in acidic electrolytes, without the help of templates or surfactants. And the Cu_2O has attracted much attention as a candidate for the anode material for lithium ion batteries (LIBs) due to several advantages, including its reversible mechanism with Li^+, its relative low-cost, and non-toxicity [14,15]. However, huge volume expansion and shrinkage, accompanying Li^+ charge and discharge processes, lead to poor charge-discharge cycle-life due to the failure of the contacts between the anode material and current collector [16,17]. Therefore, we were motivated to evaluate the Cu_2O nanorods array as an anode of LIBs because the free-volume between the nanorods would

Physical Chemistry Chemical Physics Accepted Manuscript

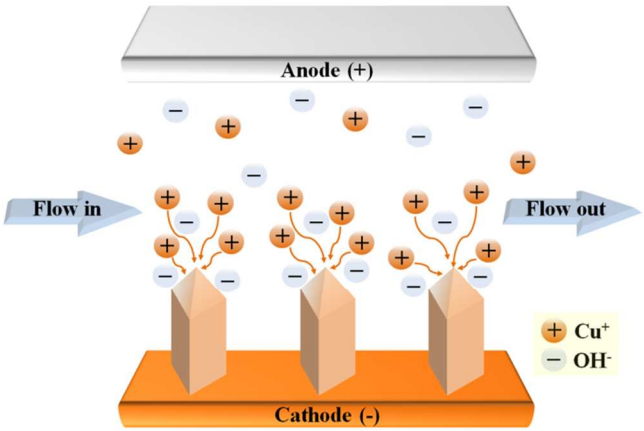

Figure 1 Schematic diagram of electrochemical flow-based solution-solid synthesis of Cu_2O nanorods array.

accommodate the huge volume changes. It was found that the Cu_2O nanorods were transformed to fragmented CuO nanoparticles and electroactive polymeric gel-like layer was generated. The nanostructures of Cu_2O and CuO including the polymeric gel-like layer had much higher electrochemical capacities than Cu_2O film structure.

2 Experimental Section

Cu_2O nanorods array was synthesized by a potentiodynamic electrodeposition process in a flowing electrolyte without any templates or surfactants (Figure 1). The electrodeposition was conducted using a two-electrode system (Solartron 1280z) at room temperature. The working electrodes were Cu foils or Au (100 nm)/Ti (10 nm) coated Si substrates. The Au and Ti films were sputter-deposited on Si substrates. The exposed area of the working electrode was 1.2 cm x 1.2 cm. Pt wire (Aldrich) was used as a counter electrode. The distance between the electrodes was 3 cm. The aqueous electrolyte was composed of 50 μM $CuSO_4 \cdot H_2O$ (Junsei Co., Japan) in deionized water. The electrolyte was injected into the rectangular bath (cross-sectional area of 3 cm x 3 cm and length of 15 cm) at a constant flow rate of 2 $L \cdot min^{-1}$ by a peristaltic pump (GP 600, Dongseo Science Co.) and flowed out of the bath. The pH and ionic conductivity of the electrolyte were 5.6 and 13 $\mu S \cdot cm^{-1}$, respectively. The frequency and duty of the potentiodynamic reverse-pulse was 0.5 Hz and 50 %, respectively. In the potentiodynamic mode, the reduction potential (V_R) and oxidation potential (V_O) were set to be -14 V and 0.5 V, respectively. In order to electrodeposit Cu nanorods array, the pH was decreased to 4.3 by adding small amount (100 μM) of H_2SO_4 into the 50 μM $CuSO_4 \cdot H_2O$ electrolyte.

The electrochemical performance of Cu_2O nanorods as an anode of LIBs was investigated using a 2032-type coin cell. The Cu_2O nanorods were directly grown on a Cu foil (18 μm in thickness, 99.8 at%, Nippon Foil Mfg Co.). Li metal foil

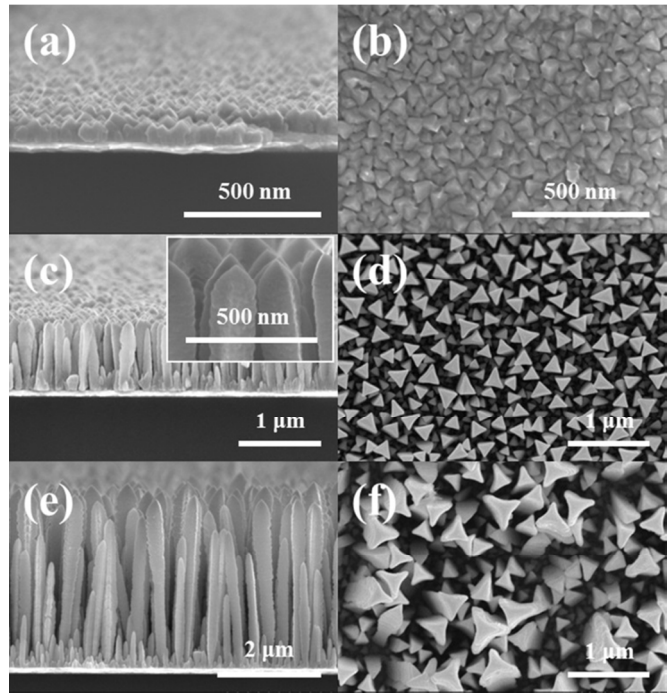

Figure 2 Cross-sectional and top-view SEM images of (a), (b) Cu_2O buffer layer, (c), (d) Cu_2O nanorods grown for 4 hours, and (e), (f) Cu_2O nanorods grown for 10 hours, respectively. The inset indicates the higher magnified image.

and microporous polypropylene (Celgard 2400) were used as a counter electrode and a separator, respectively. The electrolyte in the coin cell was 1 M $LiPF_6$ in a 1:1 (v/v ratio) mixture of ethylene carbonate and diethyl carbonate (Techno Semichem Co.). The weight of the Cu_2O nanorods was measured using a microbalance (Satorius, model 3.6P) before and after the electrodeposition. The electrochemical measurements were carried out using a multi-channel potentiostat/galvanostat (VMP3, Biologic) in the voltage ranges of 0.001 to 3.0 V. The cells were charged and discharged at a current rate of 0.1 $A \cdot g^{-1}$ (equal to 0.266 C, 1 C = 375 $mA \cdot g^{-1}$ for Cu_2O) in a galvanostatic mode. The cyclic voltammetry (CV) measurements were carried out at a scan rate of 0.1 $mV \cdot s^{-1}$.

The morphological and structural changes of the Cu_2O nanorods were analyzed using X-ray diffraction (XRD, Cu-Kα, Bruker D8), a field emission scanning electron microscope (SEM, Hitachi S4800), field emission transmission microscope (TEM, FEI Tecnai F30). For the TEM characterization, the Cu_2O nanorods were dispersed in ethanol using a sonication and a droplet containing the nanorods were dropped and dried on the lacey carbon TEM grid.

3 Results and discussion

Figures 2(a) and 2(b) show typical cross-sectional and top-view SEM images of a Cu_2O layer of 70 nm thickness (hereafter, called a Cu_2O buffer layer) electrodeposited on the Au/Ti coated Si substrates using a reverse-pulse

Physical Chemistry Chemical Physics Accepted Manuscript

This journal is © The Royal Society of Chemistry 2014

potentiodynamic process for 30 minutes. The triangular pyramid Cu_2O grains were densely deposited on the substrate. The uniform-sized grains were formed by the repeated generation and dissolution of Cu_2O nuclei during the periodic application of V_R and V_O, as discussed in the previous work [5]. A high reduction potential (V_R of -14 V) was used to overcome the low electrical conductivity (13 $\mu S \cdot cm^{-1}$) of the dilute electrolyte. Figures 2(c) and 2(d) show the typical cross-sectional and top-view SEM images of the Cu_2O nanorods electrodeposited for 4 hours. Cu_2O nanorods with a length of 1 μm and an effective diameter of about 150 nm grew perpendicular to the substrate. The Cu_2O nanorods had the shape of a triangular column with a triangular pyramid on the top. The inset of Figure 2(d) shows a higher magnified SEM image of the triangular vertex on the top. The further growth of Cu_2O nanorods, up to 4 μm in length, was observed with further deposition time up to 24 hours in the cross-sectional SEM image of Figure 2(e), while the lateral growth was effectively suppressed, as shown in the top-view SEM images of Figure 2(f). To investigate the effects of electrolyte pH and concentration on the growth of Cu_2O nanorods, sequential experiments were performed in two electrolytes; one (pH of 13.4) with a higher concentration of 0.2 M $CuSO_4$, 0.2 M tartaric acid, and 3 M NaOH, and the other (pH of 12.2) with a lower concentration of 2 μM $CuSO_4$, 2 μM tartaric acid, and 30 μM NaOH, respectively, at the reduction potential of -1 V for one hour. Results showed that Cu_2O dense films were deposited in the pH range of 12.2 to 13.4 regardless of the electrolyte concentration (see Figure S1(a) and S1(b)), implying that the growth of the nanorods might be related to the high reduction potential in the ultra-dilute electrolyte. Figure 3 shows the typical XRD patterns of the Cu_2O buffer layer and Cu_2O nanorods grown on Au/Ti coated Si substrate, respectively. The buffer layer had a strong [111]-preferred orientation, as the only strong peak was indexed to be the (111) plane of cubic Cu_2O with a lattice constant of a = b = c = 4.267 nm (JCPDS #78-2076). The other peaks came from the Si substrate and Au layer. For the Cu_2O nanorods, three diffraction peaks were indexed to be Cu_2O (111), (200) and (220) planes, in sequence. The strongest peak intensity of the (111) plane indicated the [111]-preferred orientation of the buffer layer and nanorods normal to entire substrate. Similarly, the Cu_2O nanorods with [111]-longitudinal direction were grown on Cu foil, according to the SEM and XRD analyses (See Figure S2).

It should be noted that the Cu_2O nanorods array was deposited in acidic electrolyte (pH 5.6), as shown in Figure 2 and Figure 3. The formation of Cu_2O phase in acidic electrolyte was contradictory to what is expected from the Pourbaix diagram of the Cu-water system [13]; Cu_2O is favorably deposited in alkaline electrolyte, according to the following reactions,

$$2Cu^{2+} + 2OH^- + 2e^- \rightarrow 2Cu(OH) \qquad \text{Eq.(1a)}$$

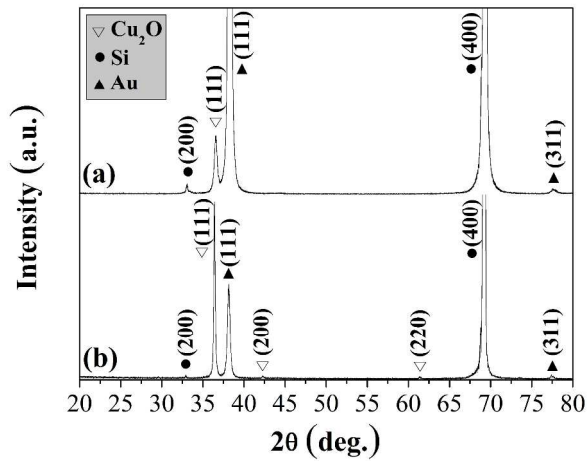

Figure 3 XRD patterns of Cu_2O buffer layer and Cu_2O nanorods.

$$2Cu(OH) \rightarrow Cu_2O + H_2O \qquad \text{Eq.(1b)}$$

In alkaline electrolyte, copper hydroxide is initially formed by the reaction of Eq.(1a) and subsequently undergoes a dehydration process via Eq.(1b) [18]. Since the formation of Cu_2O cannot in principle occur in the acidic electrolyte, the resulting growth of Cu_2O might be due to the local increase of pH near the cathode [19]. That is, the following two reactions are reasonably supposed to occur near the cathode.

$$O_2 + 2H_2O + 4e^- \rightarrow 4OH^- \qquad \text{Eq.(2a)}$$

$$2H_2O + 2e^- \rightarrow H_2 + 2OH^- \qquad \text{Eq.(2b)}$$

As the oxygen solubility in a deionized water is approximately 1 mM at room temperature, sufficient oxygen might be reduced to OH^- on the cathode, according to the O_2 gas dissolution of Eq.(2a) [20]. Thus, the generation of OH^- can contribute to increasing the local pH near the cathode and as a source for forming the copper hydroxide. In addition, water decomposition may enhance the local pH increase by increasing OH^- concentration on the cathode according to Eq.(2b) at a V_R of 14 V [21]. However, the oxygen dissolution reaction might be the more dominant contribution to the formation of the Cu_2O phase because water decomposition could occur even in the formation of the Cu phase (see Figures S3 and S4). On the other hand, water decomposition (Eq.(3)) can occur at the anode [21].

$$2H_2O \rightarrow O_2 + 4H^+ + 4e^- \qquad \text{Eq.(3)}$$

The competition of water decompositions on both the cathode and anode leads to a pH decrease for the whole electrolyte due to charge equalization, which agrees with our experimental results, that the pH of the electrolyte decreased from 5.6 to 4.9 after the growth of Cu_2O NRs.

In order to suppress oxygen dissolution (Eq.(2a)) into the electrolyte, the same electrodeposition was performed in a

Physical Chemistry Chemical Physics Accepted Manuscript

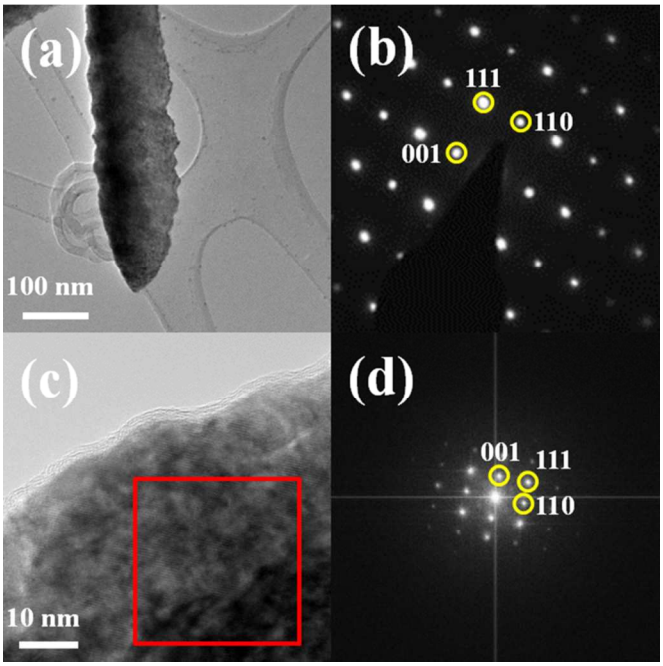

Figure 4 (a) Bright-field TEM image of a single Cu_2O nanorod, (b) electron diffraction pattern of Cu_2O nanorod corresponding to the whole nanorod shown (a), (c) high-resolution TEM image of a Cu_2O nanorod, and (d) FFT image of the square-marked area shown in (c)

glove box filled with N_2 gas. It was observed that vertical Cu nanorods with the lattice constant of a = b = c = 3.615 nm (JCPDS #4-836) were grown (Figure S3). The Cu nanorods grew along the [111]-longitudinal direction, as confirmed by XRD analyses. The results indicate that sufficient dissolution of oxygen is necessary for the growth of Cu_2O nanorods. And when the pH of the electrolyte was decreased to 3.8 by adding 100 μM H_2SO_4 into the 50 μM $CuSO_4$ electrolyte, only Cu nanorods were vertically grown on the substrate in ambient atmosphere (Figure S4). The Cu nanorods had the [111]-longitudinal direction, as confirmed by XRD analyses, which agreed with our previous results [22]. Thus, Cu_2O and Cu nanorods were selectively synthesized by controlling the pH and the oxygen dissolution in the electrolytes. Figures 4(a) and 4(b) show a typical bright field (BF) TEM image, and a corresponding selected area electron diffraction (SAED) pattern, respectively, of a Cu_2O nanorod shown in Figure 2(c). The sharp tip on the edge indicated a triangular pyramid on the top of the triangular column shown in Figure 2(c). The SAED pattern shows that the single crystalline Cu_2O nanorods grew along the [111]-longitudinal direction with a [1$\bar{1}$0]-zone axis. This result was in good agreement with the XRD analysis that Cu_2O nanorods had a strong [111]-preferred orientation. Figure 4(c) shows a typical high-resolution (HR) TEM of a Cu_2O nanorod with an amorphous layer of approximately 3 nm thickness at the surface. According to XPS analysis of O 1s and Cu 2p binding energies, Cu_2O and CuO phases co-existed at the surface of the nanorods (Figure S5). As the Gibbs free energy change

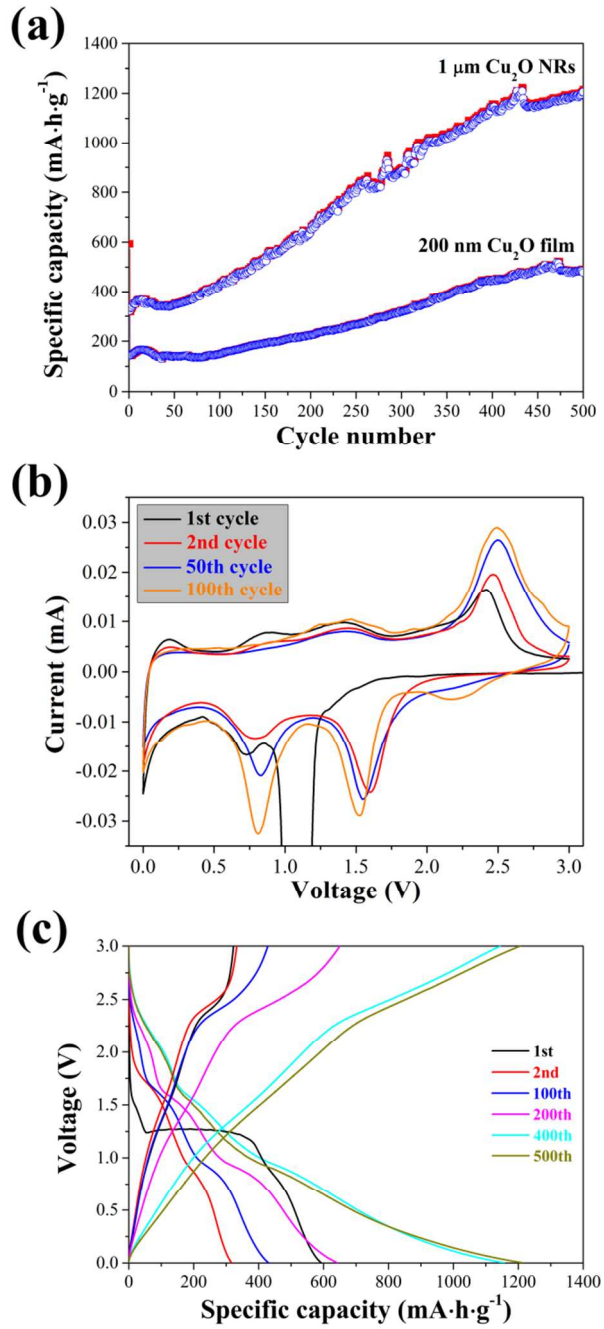

Figure 5 (a) Variations of specific capacity of 200 nm -thick Cu_2O film and Cu_2O nanorods with the cycle number of discharge/charge cycling, (b) cyclic voltammogram of Cu_2O nanorods during 100 cycles, (c) discharge/charge profiles of Cu_2O nanorods during 500 cycles.

for the solid state reaction of $Cu_2O_{(s)} + 1/2O_2 \rightarrow CuO_{(s)}$ is given as -95.9 kJ/mol at room temperature [23], the spontaneous surface oxidation of Cu_2O nanorods might occur. Figure 4(d) shows the Fast Fourier Transform (FFT) image of the square-marked area shown in Figure 4(c). The

Physical Chemistry Chemical Physics Accepted Manuscript

This journal is © The Royal Society of Chemistry 2014

Journal Name RSCPublishing

ARTICLE

FFT image is consistent with the SAED result of Figure 4(b). The three surfaces of the triangular column are composed of {110} planes and the three surfaces of the triangular pyramid on the top comprised the {100} planes. At the moment, it is not clear why the triangular pyramidal growth occurs. According to the thermodynamic equilibrium model of the Cu_2O crystal, the surface energies (γ) are in the order of (100) > (110) > (111) [24]. It was previously reported that four-faced pyramid Cu_2O films had the [100]-preferred orientation because the (111) plane, with its lowest surface energy, is the most stable and that the growth direction of the Cu_2O film was kinetically controllable by the deposition parameters such as deposition current, reduction potential and pH of electrolyte [25-27]. Thus, it is presumed that the triangular growth of [111]-longitudinal Cu_2O might be related to the nonequilibrium kinetics caused by the high reduction potential. The one-dimensional growth of Cu_2O nanorods was closely related to the electric field enhancement on the sharp tips (Figure 4(a)) which served as an anisotropic growth site, as discussed in the previous work [5]. Thus, the electrochemical flow-SS growth mechanism of Cu_2O nanorods is schematically described in Figure 1. When triangular pyramid Cu_2O grains are densely deposited on the substrate during the periodic application of V_R and V_O (shown in Figure 2(a)), the electric field in the flow of dielectric electrolyte generates a directional anisotropy on a triangular pyramid of the top, playing a role of catalyst in SLS growth. The electric field directs the Cu cations toward the pyramidal tips and the cations react with OH^- anions in the electrolyte to form Cu_2O phase. And the oxygens from the ambient are supplied to the electrolyte. With further deposition time, the Cu_2O triangular nanorods grow longer with the inflow of precursor source in the dilute electrolyte. The present electrochemical flow-SS growth is similar to the flow-based SLS synthesis reported in the literature [4], except that the electric field between the anode and the cathode replaces the role of the catalysts in flow-based SLS growth.

The electrochemical properties of Cu_2O nanorods array as an anode of LIBs were investigated by measuring the discharge and charge capacities during 500 cycles; two types of anode were prepared; Cu_2O nanorods array with a length of 1 μm (Figure 2(c)) and Cu_2O films with thicknesses of 200 nm (Figures S1(a)). The charge capacity of the 200 nm-thick films was 145 $mA{\cdot}h{\cdot}g^{-1}$ for the first cycle and gradually increased up to 479 $mA{\cdot}h{\cdot}g^{-1}$ after 500 cycles, as shown in Figure 5(a). The increase of charge capacity might be presumed to be due to the reversible phase transformation of Cu_2O to CuO during the discharge and charge cycles. And it was reported that Cu_2O nanoparticles reversibly stored the Li^+ and the extra charge capacity was generated by the decomposition of the Li-electrolyte, which makes an electrochemically active polymeric gel-like film [28]. As shown in Figure 5(a), the Cu_2O nanorods array exhibited much more excellent cycle performance of charge capacity up to 500 cycles; the charge capacity increased from 323 to 1206 $mA{\cdot}h{\cdot}g^{-1}$ during 500 cycles. The capacity value is approximately several times higher than the theoretical capacity (375 $mAh{\cdot}g^{-1}$) of Cu_2O and that (674 $mAh{\cdot}g^{-1}$) of CuO. To further understand the enhanced results, the cyclic voltammetry (CV) profiles of the Cu_2O nanorods were analyzed, as shown in Figure 5(b). During the first cycle, two cathodic reaction peaks appeared at 0.7 V and 1.1 V, while two sharp cathodic peaks were observed at 0.8 V and 1.5 V during the following cycles. The peaks corresponded to the growth reaction of the electrochemically active polymeric gel-like film, which might comprise LiF, Li_2CO_3, alkyl carbonates lithium salts ($ROCO_2Li$), and the decomposition reaction of Cu_2O nanorods into Cu-Li_2O composites, respectively [28-31]. After the first cycle, higher shifts of the cathodic reaction potentials from 1.1 to 1.5 V were associated with the structural fragmentation of the crystalline Cu_2O nanorods [28]. Since the Cu_2O nanorods were transformed to Cu/Li_2O nanocomposites during the lithiation, the electrochemically driven fragmentation of Cu_2O nanorods into nanoparticles enhanced the reactivity with Li^+. In addition, two anodic reaction peaks appeared at 1.5 and 2.5 V with further cycles. This reflected the decomposition of the polymeric gel-like film and the transformation of Cu-Li_2O composite to Cu_2O, respectively. Li_2CO_3 and alkyl carbonate lithium salts were known to be reversibly decomposed during the charge process [30]. During the 100th cycle, a new anodic reaction peak appeared around 2.8 V, and a cathodic reaction peak newly appeared around 2.2 V. The peaks were attributed to the redox reaction of CuO and Cu_2O [31,32]. Therefore, it is presumed that Cu_2O was gradually converted into a CuO phase during the further discharge and charge cycling. Figure 5(c) shows the galvanostatic discharge/charge profiles of the Cu_2O NRs during 500 cycles. With the cycle number increasing up to 500, the three discharge slopes (2.5 to 1.6 V, 1.6 to 1.0 V, and 1.0 to 0.001 V) clearly appeared, which were in good agreement with the CV results shown in Figure 5(b). It was noted that, below 1.0 V, the discharge capacity, which was closely related to the polymeric gel-like film, increased more than that in the ranges of 1.0 to 1.6 V and 1.6 to 2.5 V, respectively, which was attributed to the reactions of CuO to Cu_2O as well as Cu_2O to Cu and Li_2O. The discharge capacity above 2.2 V increased gradually when the cycles were more than 100. It agreed with the CV results that a new peak appeared at 2.8 V, due to the redox reaction of CuO and Cu_2O.

Physical Chemistry Chemical Physics Accepted Manuscript

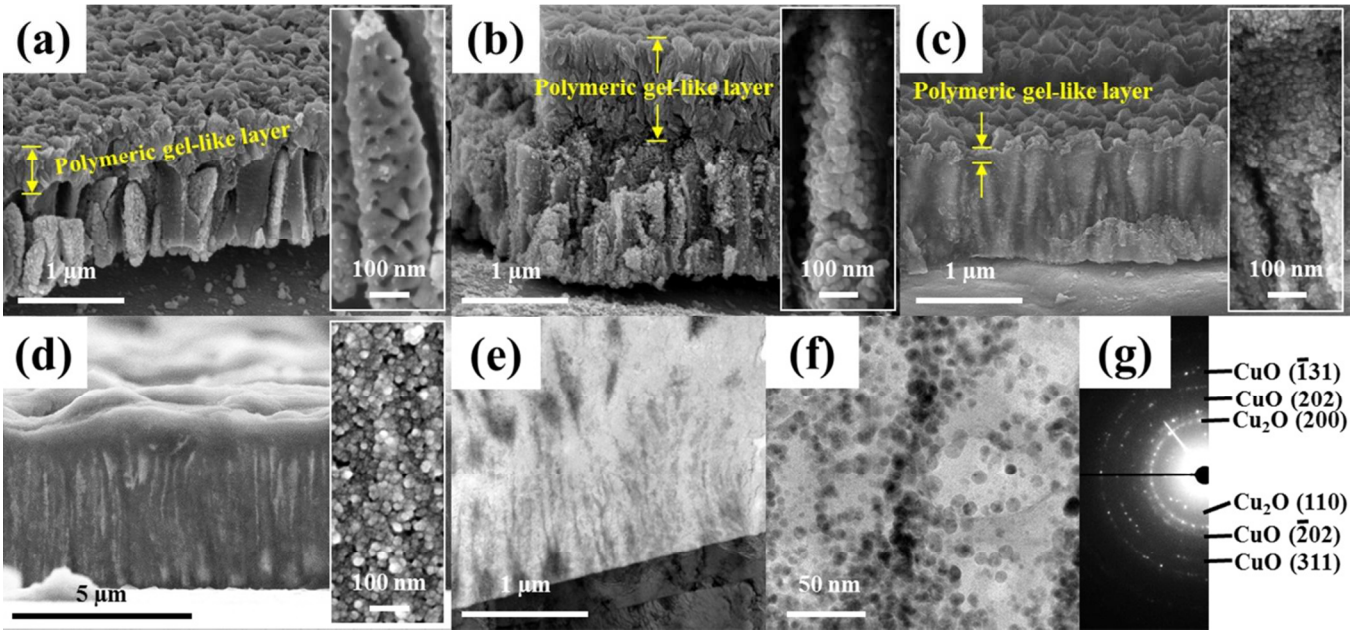

Figure 6 Morphological changes of Cu_2O nanorods with the discharge/charge cycling, after (a) the first discharge process, (b) 200th discharge process, (c) 200th charge process, (d) 400th discharge process. All insets of (a)-(d) indicate higher-magnified images. (e) BF TEM image after 400th charge process, (f) high-magnified BF TEM image of Figure 4(e), (g) SAED pattern of Figure 4(f).

Figure 6 shows the typical morphological changes of the nanorods anode with discharge/charge cycling up to 400 cycles. In Figure 6(a), the cross-sectional SEM image shows that, after the first discharge, polymeric gel-like layers with a few hundred nanometers in thickness formed at the top of the nanorods as well as between the nanorods, and that the surfaces of the Cu_2O nanorods became nanoporous, as shown in the highly magnified SEM image in the inset. As discussed above, the morphological changes of Cu_2O nanorods supported the increase of cathodic reaction potentials shown in Figure 5(b) because the nanoporosity was able to enhance the reactivity with Li^+. Figure 6(b) shows cross-sectional SEM images of the nanorods after the 200th discharge, and illustrates that the free volume between the nanorods was filled with a polymeric gel-like layer, and that a thicker polymeric gel-like layer formed on the top of the nanorods. Although the nanorod structures were apparently maintained, the nanorods were composed of nanoparticles with a size of 30 to 50 nm, as shown in the inset. In Figure 6(c), it was noted that the thickness of the polymeric gel-like layer at the top of the nanorods remarkably decreased after the 200th charge. This implies that the formation and decomposition of the polymeric gel-like film reversibly occurred during the discharge-charge processes and contributed to the increase of the electrochemical capacities, as shown in Figure 5(a). The components of the polymeric gel-like films during the discharge and charge processes after 200-cycles were analyzed and determined to be Li_2CO_3, Li_3PO_4, and LiF by XPS depth profiles (see Figure S6). For the surface of the 200th discharge sample (Figure S6(a)), the single C 1s peak, corresponding to Li_2CO_3, was detected at 289.8 eV. An Ar^+ ion milling process was performed to analyze the depth profile of composition, although the milling time was not calibrated to the depth. F 1s and P 2p emission lines, corresponding to LiF and Li_3PO_4, appeared at the Ar^+ ion milling time of 60 and 150 minutes, respectively. In contrast, the P 2p emission line was not detected after the 200th charge process (Figure S6(b)), while the C 1s and F 1s spectra appeared continuously with the ion milling times. Therefore, it is reasonably supposed that the thick polymeric layer at the top surface as well as between the NRs was mainly composed of Li_2CO_3 including a small amount of LiF after the 200th discharge process, and that the Li_3PO_4 existed only between the NRs after the discharge process. The thinner polymeric layer after the 200th charge process indicated that a large amount of Li_2CO_3 at the top surface was decomposed. When comparing the F 1s emission lines after discharge and charge processes, the LiF, most of which was not decomposed, existed at the bottom of the thick polymeric layer as well as between the NRs. It was noted that Li_3PO_4 between the NRs was completely decomposed during the charge process. Thus, it is reasonably presumed that the formation and decomposition of Li_3PO_4 is reversible while those of LiF are irreversible. However, some Li_2CO_3 was irreversibly formed on the top surface of the NRs. Figure 6(d) shows the cross-sectional SEM image of the NRs after 400th charge. The length of NRs increased up to 4 μm from the initial length of 1 μm. The nanorod structures were composed of fragmented nanoparticles (10 to 20 nm in size). The polymeric gel-like layers fully penetrated in between of the NRs and become thicker on the NRs surface, to approximately 1 μm, in comparison to the thickness (several hundred nanometers) shown in Figure 6(c). In Figure 6(e), the typical bright field (BF) TEM image of NRs after the 400th charge process shows that the nanoparticles were

Physical Chemistry Chemical Physics Accepted Manuscript

This journal is © The Royal Society of Chemistry 2014

fragmented and embedded in a polymeric gel-like matrix. As shown in the highly-magnified BF TEM image of Figure 6(f), the NRs completely transformed to nanoparticles (approximately 10 nm in size) within the polymeric matrix. The nano-sized fragmentation of the NRs proceeded with repeating of the discharge and charge processes. Figure 6(g) shows the SAED pattern corresponding to the image of Figure 6(f). The polycrystalline ring patterns were indexed to be Cu_2O and CuO. This supports the gradual phase transformation of Cu_2O to CuO phase during longer discharge and charge cycling.

The mechanism of gradually increasing electrochemical capacity of Cu_2O nanorods is summarized; during the first discharge process, the nanorods are transformed to a porous nanorod structure and the thick electroactive gel-like polymer layer is formed on the top surface of the nanorods as well as between the nanorods. During the following charge process, the electroactive polymeric layers are reversibly decomposed at the top surface. With repeating cycles of discharge-charge processes, the nanorods are structurally transformed to fragmented nanoparticles, the phase of which are transformed from Cu_2O to CuO, causing the enhancement of surface activity and increasing the charge capacity [33]. Simultaneously, the thickening of the top electroactive polymer layer and the penetration of the electroactive polymer into the inbetween of the fragmented nanoparticles contribute to the more enhancement of the electrochemical capacity. The remarkable enhancement of life cycle is attributed to the electroactive polymeric gel-like matrix which serves as a buffer against the large volume expansion related to the lithiation of fragmented nanoparticles [34].

4 Conclusions

The electrochemical flow-SS growth of single-crystalline Cu_2O nanorods array was successfully realized under the electrochemical flow of dielectric electrolyte. The nanorods growth originated from the directional anisotropy caused by the electric field enhancement on the triangular pyramidal grains in the ultra-dilute aqueous electrolyte. The selective growth of Cu_2O and Cu nanorods in the acidic electrolyte was demonstrated by controlling the pH and the oxygen dissolution into the electrolyte. The Cu_2O nanorods array was proved to be a potential candidate as an anode material for LIBs with electrochemical capacities gradually increasing from 323 to 1206 $mA{\cdot}h{\cdot}g^{-1}$ during 500 cycles. The outstanding enhancement of the capacities was attributed to a phase transformation from Cu_2O to CuO, accompanying a nano-restructuring from nanorods to fragmented nanoparticles and the progressive generation of electroactive polymeric gel-like films. The electrochemical flow-SS growth in dielectric electrolyte is expected to be utilized as a facile, environment-friendly, mass production, and low-cost method for developing other functional nanorods array.

Acknowledgements

We would like to acknowledge the financial support from the R&D Convergence Programs of MSIP (Ministry of Science, ICT and Future Planning) and ISTK (Korea Research Council for Industrial Science and Technology, Grant B551179-13-01-03), and KRCF (Korea Research Council of Fundamental Science and Technology, Grant 13-2-KIST) of Republic of Korea.

Notes

[a] *Center for Nanomaterials Characterization, Korea Research Institute of Standards and Science, Daejeon, 305-340, Republic of Korea. *E-mail: jysong@kriss.re.kr*
[b] *Division of Nano-mechanical Systems Research, Korea Institute of Machinery and Materials, Daejeon, 305-343, Republic of Korea.*
[c] *Korea University of Science and Technology, Daejeon 305-350, Republic of Korea*

†Electronic Supplementary Information (ESI) available [Additional results on SEM images, XRD and XPS of Cu nanorods and Cu_2O films]. See DOI: 10.1039/b000000x/.

References

[1] R. S. Wagner, W.C. Ellis, *Appl. Phys. Lett.* 1964, **4**, 89.
[2] T. J. Trentler, K. M. Hickman, S. C. Goel, A. M. Viano, P. C. Gibbons, W.E. Buhro, *Science* 1995, **270**, 1791.
[3] F. Wang, A. Dong, J. Sun, R. Tang, H. Yu, and W.E. Buhro, *Inorg. Chem.* 2006, **45**, 7511.
[4] R. Laocharoensuk, K. Palaniappan, N.A. Smith, R. M. Dickerson, D. J. Werder, J. K. Baldwin, and J. A. Hollingsworth, *Nat. Nanotech*. 2013, **8**, 660.
[5] S. H. Park, H. S. Shin, Y. H. Kim, H. M. Park, J. Y. Song, *Nanoscale* 2013, **5**, 2029.
[6] K. Akimoto, S. Ishizuka, M. Yanagita, Y. Nawa, G. K. Paul, T. Sakuri, *Solar Energy* 2006, *80*, 715.
[7] M. Hara, T. Kondo, M. Komoda, S. Ikeda, K. Shinohara, A. Tanaka, J. N. Kondo, K. Domen, *Chem. Commun*. 1998, **3**, 357.
[8] J. Zhang, J. Liu, Q. Peng, X. Wang, Y. Li, *Chem. Mater*. 2006, **18**, 867.
[9] D. P. Singh, N. R. Neti, A. S. K. Sinha, O. N. Srivastava, *J. Phys. Chem. C* 2007, **111**, 1638.
[10] D. Barreca, A. Gasparotto, C. Maccato, E. Tondello, O. I. Lebedev, G. V. Tendeloo, *Cryst. Growth Des*. 2009, **9**, 2470.
[11] W. Wang, G. Wang, X. Wang, Y. Zhan, Y. Liu, C. Zheng, *Adv. Mater*. 2002, **14**, 67.
[12] Y. Tan, X. Xue, Q. Peng, H. Zhao, T. Wang, Y. Li, *Nano Lett.* 2007, **7**, 3723.
[13] B. Beverskog, I. Puigdomenech, *J. Electrochem. Soc*. 1997, **144**, 3476.
[14] Y. H. Lee, I. C. Leu, S. T. Chang, C. L. Liao, K. Z. Fung, *Electochim. Acta* 2004, **50**, 553.
[15] S. Bijani, M. Gabas, G. Subias, J. Garcia, L. Sanchez, J. Morales, L. Martinez, J. R. Ramos-Barrado, *J. Mater. Chem*. 2011, **21**, 5368.
[16] K. Chen, D. Xue, *Cryst. Eng. Comm*. 2013, **15**, 1739.
[17] A. Lamberti, M. Destro, S. Bianco, M. Quaglio, A. Chiodoni, C. F. Pirri, C. Gerbaldi, *Electrochim. Acta* 2012, **70**, 62.
[18] H. S. Shin, J. Y. Song, J. Yu, *Mater. Lett*. 2009, **63**, 397
[19] J. Y. Lee, Y. S. Tak, *Electrochem. Solid State Lett*. 1999, **2**, 559

Physical Chemistry Chemical Physics Accepted Manuscript

[20] K. Kinoshita, *Electrochemical Oxygen Technology*, Wiley, New York, 1992.
[21] D. A. Jones, *Principles and Prevention of Corrosion*, 2nd Ed., Prentice Hall, 1995
[22] S. H. Park, H. S. Shin, Y. H. Kim, H. M. Park, J. Y. Song, *J. Alloys Comp*. 2013, **580**, 152.
[23] R. L. David, *Handbook of Chemistry and Physics*, 76th ed., New York, CRC press, 1995-1996.
[24] Z. Zheng, B. Huang, Z. Wang, M. Guo, X. Qin, X. Zhang, P. Wang, Y. Dai, *J. Phys. Chem. C* 2009, **113**, 14448.
[25] T. Shinagawa, Y. Ida, K. Mizuno, S. Watase, M. Watanabe, M. Inaba, A. Tasaka, M. Izaki, *Cryst. Growth Des.* 2013, **13**, 52.
[26] L. C. Wang, N. R. D. Tacconi, C. R. Chenthamarakshan, K. Rajeshwar, M. Tao, *Thin Solid Films* 2007, **515**, 3090.
[27] Y. H. Lee, I. C. Leu, C. L. Liao, K. Z. Fung, *J. Alloys Comp.* 2007, **436**, 241.
[28] C. Q. Zhang, J. P. Tu, X. H. Huang, Y. F. Yuan, X. T. Chen, F. Mao, *J. Alloys Comp*., 2007, **441**, 52.
[29] P. Balaya, H. Li, L. Kienle, J. Maier, *Adv. Funct. Mater.* 2003, **13**, 632.
[30] B. Laik, P. Poizot, J. M. Tarascon, *J. Electrochem Soc*. 2002, **149**, A251.
[31] J. Morales, L. Sánchez, F. Martín, J. R. Ramos-Barrado, M. Sánchez, *Thin Solid Films* 2005, **474**, 133.
[32] X. P. Gao, J. L. Bao, G. L. Pan, H. Y. Zhu, P. X. Huang, F. Wu, D. Y. Song, *J. Phys. Chem. B* 2004, **108**, 5547.
[33] O. S. Ivanova, F. P. Zamborini, *J. Am. Chem. Soc*. 2010, **132**, 70.
[34] S. R. Gowda, A. L. M. Reddy, M. M. Shaijumon, X. Zhan, L. Ci, P. M. Ajayan, *Nano Lett.* 2011, **11**, 101.

Physical Chemistry Chemical Physics Accepted Manuscript

This journal is © The Royal Society of Chemistry 2014